Available online at www.sciencedirect.com
SCIENCE DIRECT
Journal of Photochemistry and Photobiology A: Chemistry 176 (2005) 98–106
Journal of Photochemistry and Photobiology A:Chemistry
www.elsevier.com/locate/jphotochem

UV absorption spectra of methyl-substituted hydroxy-cyclohexadienyl radicals in the gas phase

David Johnson [a,1], Séverine Raoult [a], Robert Lesclaux [a,*], Lev N. Krasnoperov [b]

[a] *Laboratoire de Physico-Chimie Moléculaire, UMR 5803 CNRS, Université Bordeaux I, 33405 Talence Cedex, France*
[b] *Department of Chemistry and Environmental Science, New Jersey Institute of Technology, University Heights, Newark, NJ 07102, USA*

Available online 21 October 2005

Abstract

UV absorption spectra of five methyl-substituted hydroxy-cyclohexadienyl radicals, formed by the addition of the hydroxyl radical (OH) to toluene (methyl benzene), *o*-, *m*- and *p*-xylene (1,2-, 1,3- and 1,4-dimethyl benzene, respectively) and mesitylene (1,3,5-trimethylbenzene), have been determined at 298 K, 1 atm pressure ($N_2 + O_2$), and the corresponding absolute absorption cross-sections measured, using laser flash photolysis and time-resolved UV absorption detection. As observed for other cyclohexadienyl-type radicals, a strong absorption band is present in the 260–340 nm spectral region, with maximum cross-sections in the range $(0.9–2.2) \times 10^{-17}$ cm^2 molecule^{-1}. The shape of the band varies significantly from one radical to the next for the series of aromatic precursors investigated. The nature and yields of hydroxylated ring-retaining oxidation products, identified in previous studies of the OH-initiated oxidation of aromatic hydrocarbons, and the results of theoretical density functional theory (DFT) calculations indicate that one or more possible isomers of the various OH-adducts may contribute to the observed spectra. Isomers where the OH-group is *ortho*- (or both *ortho*- and *ipso*-) to a substituent methyl-group are likely to be the most abundant but other isomers may also be formed to a significant extent. Nonetheless, the present study provides absorption spectra of the adduct radicals formed from the gas phase addition of OH to the aromatic hydrocarbons considered, near room temperature and 1 atm pressure.

Keywords: Hydroxy-cyclohexadienyl radicals; UV absorption spectra

1. Introduction

Cyclohexadienyl-type radicals are important reactive intermediates in reaction systems involving aromatic hydrocarbons. They generally result from the addition of radical species (including atoms) to C_6 aromatic rings. They exhibit strong resonance stabilisation as a result of five-electrons in a cyclic π-system, and this confers upon them specific reactivity and spectroscopic properties.

UV absorption spectra of cyclohexadienyl-type radicals (hereafter denoted as X-CHD or, in the case of the radicals of interest in the present work, aromatic-OH-adduct radicals) were first measured in the condensed-phase using pulsed radiolysis. Several spectroscopic studies have been reported in the literature. For example, Sauer and Mani [1] identified the absorption spectra of various X-CHD radicals, along with radicals resulting from larger aromatic systems. In general, the spectra are characterised by a strong absorption band situated in the 260–350 nm wavelength region exhibiting either a single or several peaks.

In the gas phase, absorption spectra have mostly been reported for the cyclohexadienyl radical, *c*-C_6H_7 (i.e. *c*-C_6H_6-H adduct) [2–4], and for the hydroxy-cyclohexadienyl radical, *c*-C_6H_6-OH [4–6]. The *c*-C_6H_7 spectrum exhibits a single sharp band peaking at 302 nm ($\sigma_{302\,nm} = 2.55 \times 10^{-17}$ cm^2 molecule^{-1}) [4], whereas the *c*-C_6H_6-OH spectrum, determined by two independent measurements [5,6], is broader with a main band peaking around 280–285 nm ($\sigma = 0.8 - 1.0 \times 10^{-17}$ cm^2 molecule^{-1}) and a shoulder at 310–320 nm. The absorption cross-sections, including those measured at a single wavelength [7,8] are in reasonable agreement, the observed differences are within experimental uncertainties. The relative spectrum of the radical formed from the addition of OH to toluene has also been reported [2,9] and an absolute cross-section has been measured at a single wavelength,

* Corresponding author. Tel.: +33 540 00 63 07; fax: +33 540 00 66 45.
E-mail address: r.lesclaux@lpcm.u-bordeaux1.fr (R. Lesclaux).
[1] Present address: School of Chemistry, University of Reading, Whiteknights, Reading RG6 6AD, UK.

1010-6030/$ – see front matter © 2005 Elsevier B.V. All rights reserved.
doi:10.1016/j.jphotochem.2005.09.016

308 nm, with $\sigma_{308\,nm} = 1.1 \times 10^{-17}$ cm^2 molecule^{-1} [10], which is about twice as large as that for *c*-C_6H_6-OH (i.e. the benzene-OH-adduct) at this wavelength. To our knowledge, no other gas phase spectra of X-CHD species have been reported.

New absorption spectra have been measured in the present investigation for methyl-substituted hydroxy-cyclohexadienyl radicals derived from the addition of OH to five aromatic compounds which are prevalent in the Earth's troposphere, viz. *c*-$C_6H_5(CH_3)$-OH (derived from toluene); 1,2-*c*-$C_6H_4(CH_3)_2$-OH (derived from *o*-xylene); 1,3-*c*-$C_6H_4(CH_3)_2$-OH (derived from *m*-xylene); 1,4-*c*-$C_6H_4(CH_3)_2$-OH (derived from *p*-xylene) and 1,3,5-*c*-$C_6H_3(CH_3)_3$-OH (derived from mesitylene). Absorption cross-sections were determined relative to the well established UV absorption characteristics of the ethylperoxy radical, $C_2H_5O_2$ [11]. Cyclohexadienyl-type radicals were generated from the laser flash photolysis of H_2O_2 (to produce OH) and subsequent addition of OH to the appropriate aromatic hydrocarbon.

2. Experimental methods

Experiments were performed using the laser flash photolysis technique for generating and monitoring radicals. The apparatus and methodology used have been described more fully elsewhere [12], and in the context of the OH-initiated oxidation of aromatic hydrocarbons in a recent paper [5], but briefly consisted of the following. OH radicals were generated from the laser flash photolysis of H_2O_2 at 248 nm, using a KrF excimer laser, and subsequent reaction of OH with the appropriate aromatic precursor yielded the hydroxy-cyclohexadienyl radical of interest. For example, in the case of toluene the reactions are:

$$H_2O_2 + h\nu\,(248\,nm) \rightarrow 2OH \quad (1)$$

$$OH + c\text{-}C_6H_5(CH_3) \rightarrow c\text{-}C_6H_5(CH_3)\text{-}OH \quad (2)$$

$$OH + c\text{-}C_6H_5(CH_3) \rightarrow c\text{-}C_6H_5(CH_2) + H_2O \quad (3)$$

The side-reaction (3), producing benzyl and methyl-substituted benzyl radicals, accounts for about 10% (*p*-xylene), 6% (toluene), 5% (*o*- and *m*-xylene) and less than 4% (mesitylene), of the total OH reaction with the methyl-substituted benzenes investigated [13]. Both benzyl and methyl-substituted benzyl radicals exhibit similar UV spectra composed of two main absorption bands at around 250 and 300 nm [9,14,15]. The band at 300 nm, which can in principle interfere with the OH-adduct spectra, is itself composed of two fairly sharp features at 295 and 305.3 nm for toluene (σ of the order of $(1–2) \times 10^{-17}$ cm^2 molecule^{-1}). However, such sharp bands did not appear clearly on the aromatic-OH-adduct spectra recorded in the present investigation, probably due to the fairly low spectral resolution used (1 nm) and to the wavelength spacing of individual measurement runs. Thus, any correction for benzyl radical contributions would not be significant and would be fairly arbitrary. Therefore, no corrections were applied to the measured spectra to account for the presence of benzyl-type radicals. However, the fractional consumption of OH radicals through reaction (3) was taken into account, using the branching ratios given above, in determining the cross-sections of the aromatic-OH-adduct species.

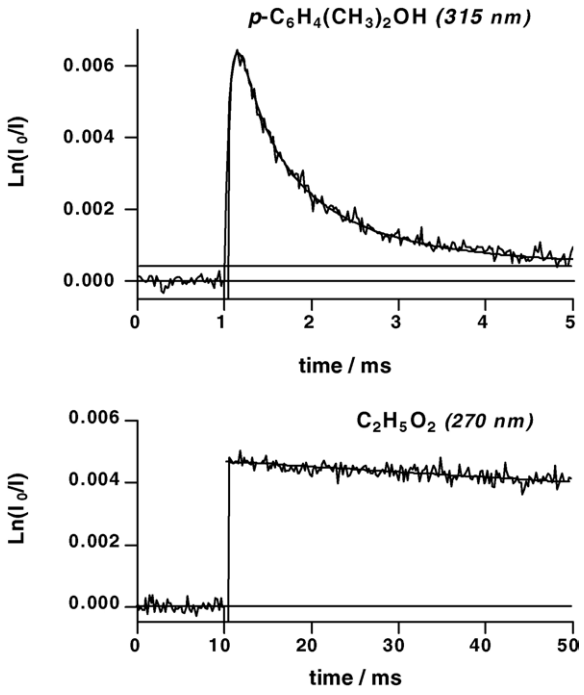

Fig. 1. Decay traces of the *p*-xylene-OH-adduct and of the $C_2H_5O_2$ radical generated with the same initial OH concentration, 1.50×10^{13} molecule cm^{-3} (optical path length: 140 cm). Solid lines are the results of simulations. The upper horizontal line, in the case of the *p*-xylene-OH-adduct, represents the base line (residual absorption, see text).

Time-resolved UV absorption signals (e.g. see Fig. 1), attributable to the aromatic-OH-adducts, were recorded in the wavelength range 260–350 nm. The gas mixture, prepared using calibrated mass flow controllers, was flowed through the reactor, a cylindrical glass reaction cell (70 cm in length, 1.8 cm internal diameter and fitted with Suprasil windows).

The UV monitoring radiation was provided either by a deuterium lamp (single pass through the reaction cell, path length 70 cm) or a high-pressure xenon lamp (double pass through the cell, path length 140 cm). UV spectra were derived from absorption decay traces recorded at various wavelengths, as indicated in the tables below. A typical decay trace is given in Fig. 1 for the case of the *p*-xylene-OH-adduct. Knowing the initial OH radical concentration, decay traces were numerically simulated with a kinetic and mechanistic representation of the gas phase radical chemistry, and a non-linear least squares fitting procedure to optimally adjust the aromatic-OH-adduct absorption cross-sections, at each wavelength studied. As in previous studies [5,6,8,10,16], a residual absorption was observed after the radical decay. This was assigned to the formation of absorbing molecular photoproducts resulting from the direct excitation of the aromatic compound at 248 nm [16], since a constant absorption was obtained by excitation of the aromatic alone, in the absence of H_2O_2. In addition, the intensity of both the constant absorption and the residual absorption were the same, within uncertainties, and hence the residual absorption was taken as the baseline in the analysis of transient absorption signals.

The photolysing radiation was provided by a KrF excimer laser (Lambda Physik EMG 200), with $\lambda = 248$ nm, directed longitudinally through the cell by dichroic mirrors. The aromatic-OH-adduct concentrations were typically in the range $(2–8) \times 10^{12}$ molecule cm^{-3} for initial OH concentrations of $(4–25) \times 10^{12}$ molecule cm^{-3}, with laser fluences of 15–25 mJ cm^{-2} pulse^{-1}. For each individual measurement, at a given wavelength, 100–300 decay traces were digitally recorded and averaged to improve the signal-to-noise ratio. Sufficient time was allowed between successive laser pulses for the contents of the reaction cell to be completely replenished with reactants/radical precursors.

All experiments were carried out at 1 atm total pressure and 295 K, and gas mixtures were prepared by passing known flows of N_2 through separate bubblers containing aqueous H_2O_2 solution and the appropriate aromatic precursor (all precursors used were liquids) before being entrained by, and mixed with, a known fast flow of N_2, or N_2 and O_2. The resulting steady state concentration of H_2O_2 in the reaction cell was determined by its absorption at 210 nm ($\sigma = 3.57 \times 10^{-19}$ cm^2 molecule^{-1}) [17] and aromatic hydrocarbon concentrations were calculated from their vapour pressures (n.b. the bubbler containing the aromatic hydrocarbon was thermostatted using a bath of melting ice/water) and the fractional flow-rate passing through the bubbler containing the aromatic compound. Typically, concentrations of $(1–6) \times 10^{15}$ molecule cm^{-3} (H_2O_2) and $(2–6) \times 10^{15}$ molecule cm^{-3} (aromatic hydrocarbons) were employed in all experiments.

Hydrogen peroxide (Aldrich, 50 wt%), toluene (Aldrich, 99.8%), 1,3-dimethylbenzene (*m*-xylene) and 1,4-dimethylbenzene (*p*-xylene) (Aldrich, 99%), 1,2-dimethylbenzene (*o*-xylene) and 1,3,5-trimethylbenzene (mesitylene) (Aldrich, 98%), ethane (AGA, 99.95%), nitrogen (Messer, 99.995%) and oxygen (Messer, 99.995%) were all used without further purification. Data were processed using numerical simulations of decay traces, based on the reaction mechanism already used in the case of benzene [5,16] and detailed in Table 1 for the particular case of toluene.

3. Determination of spectra

UV spectra of OH-adducts were derived from kinetic simulations of time-resolved absorption signals (Fig. 1) and relative cross-sections were optimally adjusted at each wavelength studied. Simulations comprised a kinetic analysis of the reaction system using the same gas phase radical reaction mechanism for all compounds (albeit with different reaction rate constants for each system). This methodology is similar to that used in previous kinetic studies of the reactions of molecular oxygen with both the benzene-OH-adduct [5,6,8,16] and the toluene-OH-adduct [10]. The mechanism used in the present investigation for the reaction of OH with toluene is presented in Table 1. Adjusted parameters were the OH-adduct cross-section and, at low oxygen concentration (see Section 4), the rate constants for radical–radical reactions which were adjusted for various experimental conditions. It should be emphasised that the cross-section values derived from the simulations were not very sensitive to the rate constants used, provided the shape of the decay curve was correctly fitted. The only rate constant values that could significantly affect the determination of cross-sections are those of $(k_2 + k_3)$ and k_6, i.e. the rate constants for the initial OH reaction with the precursor and with H_2O_2, respectively, as the relative rates of these reactions determine the branching ratio for the OH reactions. However, the values of $(k_2 + k_3)$ are fairly well established for the aromatic compounds studied in the present work [13], and the kinetics of the reaction of OH with H_2O_2 has been well studied and the reported results critically evaluated [17].

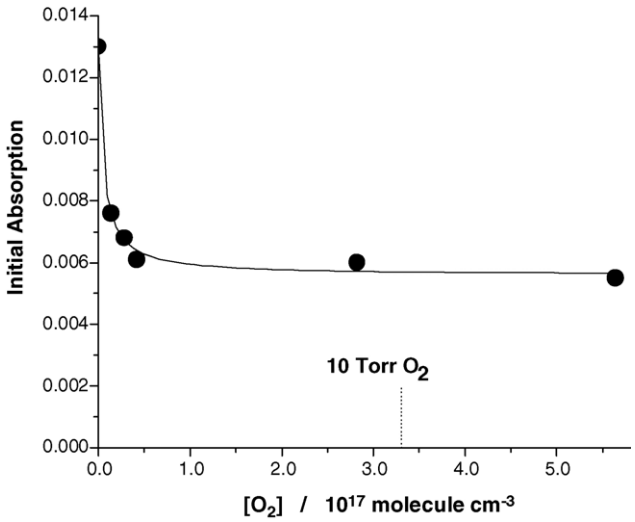

Fig. 2. Quenching of the excited toluene by molecular oxygen. Points, the amplitude of absorption of the adduct $C_6H_5(CH_3)$-OH at 320 nm. Solid line, fitting of the experimental point by a modified Stern–Volmer dependence (hyperbola with a free vertical bias). Dotted line indicates 10 Torr of molecular oxygen.

As observed in previous experiments employing laser flash photolysis to study the OH-initiated oxidation of both benzene and toluene, an additional production of OH was observed, in the absence of oxygen, which resulted from the photosensitised decomposition of H_2O_2 by the aromatic compound after excitation by the laser radiation [5,6,8,10,16]. It was further shown in these studies, and verified in the present work for other aromatic compounds, that this photosensitisation could be completely quenched by the addition of small amounts of oxygen (partial pressure 8–10 Torr). An example for the signal amplitude "quenching" by molecular oxygen for the toluene-OH-adduct is given in Fig. 2. Thus, in the present investigation, all spectra were determined in the presence of 8–10 Torr oxygen. Fig. 2 indicates that at such conditions the quenching is almost complete and that any correction for the incomplete quenching of the excited aromatic molecule would be of negligible importance. Under such conditions, the reactions of OH-adducts with oxygen (equilibrium (4,−4) and reaction (5), Table 1) only occurred to a small extent, as shown by the slowly decreasing plateau following the initial decay in Fig. 2. Nevertheless, these reactions were included in the analysis reaction mechanism. The rate constants for these latter processes have been determined in this laboratory using much higher concentrations of O_2 (the results of these studies will be reported separately).

Table 1
Reaction mechanism used for analysis of experimental signals obtained in the case of OH addition to toluene

Reaction		$k_{298\,K}$/cm^3 molecule^{-1} s^{-1} [a]	References and comments
$H_2O_2 + h\nu \rightarrow$ 2OH	(1)		
OH + $C_6H_5(CH_3)$ → c-$C_6H_5(CH_3)$-OH	(2)	5.26×10^{-12}	[13]
OH + $C_6H_5(CH_3)$ → c-$C_6H_5(CH_2)$ + H_2O	(3)	0.34×10^{-12}	[13]
c-$C_6H_5(CH_3)$-OH + O_2 → RO_2	(4) [b]	2.5×10^{-15}	Adjusted (to be published)
RO_2 → c-$C_6H_5(CH_3)$-OH + O_2	(-4)	8600 s^{-1}	Adjusted (to be published)
c-$C_6H_5(CH_3)$-OH + O_2 → Products	(5) [c]	6.0×10^{-16}	Adjusted (to be published)
OH + H_2O_2 → H_2O + HO_2	(6)	1.7×10^{-12}	[17]
OH + HO_2 → H_2O + O_2	(7)	1.1×10^{-10}	[17]
$HO_2 + HO_2$ → $H_2O_2 + O_2$	(8)	3.8×10^{-12} [d]	[23]
2c-$C_6H_5(CH_3)$-OH → Products	(9)	4.7×10^{-11}	[10]
c-$C_6H_5(CH_3)$-OH + OH → Products	(10)	1×10^{-10} [e]	Estimated
c-$C_6H_5(CH_3)$-OH + HO_2 → Products	(11)	$5–10 \times 10^{-11}$	Adjusted
c-$C_6H_5(CH_3)$-OH + RO_2 → Products	(12)	5×10^{-11}	Estimated, see reference [16]
$RO_2 + RO_2$ → Products	(13)	1.6×10^{-12} [e,f]	[24]
$RO_2 + HO_2$ → Products	(14)	2×10^{-11} [e,f]	[23]

The same mechanism, with appropriate rate constants, is used for other compounds.
[a] Other units are indicated.
[b] With R = c-$C_6H_5(CH_3)$-OH.
[c] Include reaction (5a) forming cresols and all other reaction channels leading to oxidation products.
[d] Determined for the experimental conditions prevailing in this work [24].
[e] Has a negligible influence on kinetic simulations.
[f] Value determined for peroxy radicals of similar structure.

Absolute absorption cross-section measurements were performed near to the maximum of each absorption spectrum. Experiments involved replacement of the aromatic compound with ethane to generate ethylperoxy radicals. Since the aromatic compounds absorb at the photolysis wavelength (248 nm), a small correction (<5%) was applied to account for this absorption. In order to simulate the observed transient absorption signals and to determine absorption cross-sections for the aromatic-OH-adduct species studied, it was necessary to know the initial concentration of OH radicals under the conditions of each photolysis experiment. OH concentrations were determined by calibration using the well-known absorption characteristics of the ethylperoxy radical, $C_2H_5O_2$. $C_2H_5O_2$ was generated under the same conditions of total flow-rate, H_2O_2 flow-rate, temperature and pressure using the OH + C_2H_6 (+ O_2) reaction (Fig. 1). Ethane concentrations (2–10) $\times 10^{17}$ molecule cm^{-3} were chosen such that all OH radicals were converted to $C_2H_5O_2$. The reference UV absorption spectrum of $C_2H_5O_2$ used is based upon a critical review of several determinations reported in the literature made under various experimental conditions and constitutes the most accurate spectrum presently available [11]. In addition, it is relatively easy to measure the $C_2H_5O_2$ transient absorption with precision, as the recombination rate of this radical is relatively slow and, thus, transient signals can be recorded with good signal-to-noise ratio. The $C_2H_5O_2$ absorption was observed at 270 nm (Fig. 1) where $\sigma = 2.22 \times 10^{-18}$ cm^2 molecule^{-1} for this species [11].

4. Results and discussion

Measured cross-sections are listed in Table 2 and the corresponding spectra are presented in Figs. 3–7. It can be seen that all of the spectra comprise a main absorption band in the same wavelength region, 260–340 nm, as already observed for other X-CHD radicals, and in particular for the benzene-OH-adduct [4–6]. It can also be seen that the shape of the band varies significantly from one aromatic system to the next for the series of aromatic compounds investigated. It would seem that the observed variations are related to the presence of two poorly resolved sub-bands, roughly situated at 280–300 and 310–325 nm, with different relative intensities from one compound to the next. The short wavelength band is the most intense

Table 2
Details of cross-section measurements for the OH-adducts investigated

Toluene-OH		*o*-Xylene-OH		*m*-Xylene-OH		*p*-Xylene-OH		Mesitylene-OH	
λ	σ	λ	σ	λ	σ	λ	σ	λ	σ
267	1.35	274	1.90	277	3.54	272	1.12	265	5.11
270	1.96	276	2.88	280	5.30	275	2.18	270	7.02
272	3.06	277	3.47	282	6.52	280	4.12	272	7.76
275	4.06	278	3.54	285	6.20	282	5.14	275	8.00
277	5.78	280	4.66	287	8.21	285	5.93	277	8.69
280	6.96	282	5.17	290	8.81	290	7.66	280	6.45
282	8.77	284	5.68	292	9.39	292	7.84	282	6.18
287	9.26	285	6.16	295	9.96	295	8.04	285	5.58
290	8.81	286	5.71	297	10.6	300	8.26	287	5.01
292	9.18	287	5.60	300	11.6	302	8.11	290	5.79
295	9.33	288	5.36	302	10.9	305	8.11	292	6.44
297	9.02	290	5.60	305	11.7	307	8.57	295	6.98
300	8.90	292	5.89	307	11.8	310	8.26	297	6.96
302	9.04	295	5.91	310	13.0	312	7.84	300	7.33
305	9.13	296	5.92	312	13.9	315	7.17	302	8.85
307	9.52	297	6.37	315	15.6	317	6.66	305	10.9
310	9.66	300	6.20	317	15.6	320	6.54	307	12.7
312	9.63	302	6.52	320	16.7	322	6.70	310	14.4
315	9.63	305	6.72	322	16.5	323	6.74	312	14.2
317	9.91	307	6.81	325	13.8	325	7.34	315	14.5
320	9.58	310	7.69	327	11.4	327	6.81	317	13.8
322	8.49	312	7.65	330	8.00	329	5.87	320	16.1
325	8.19	315	8.47	332	4.95	330	5.36	322	18.6
327	7.39	317	8.82	337	1.58	331	5.04	325	21.9
330	4.36	320	8.52			332	5.63	327	20.9
332	1.78	322	8.37			333	5.76	330	18.9
335	0.98	325	7.69			338	2.52	332	13.4
		327	7.00					335	8.38
		330	4.66					337	4.33
		332	2.91					340	1.94
		335	1.50						

λ, wavelength in nm; σ, cross-section in 10^{-18} cm^2 molecule^{-1}.

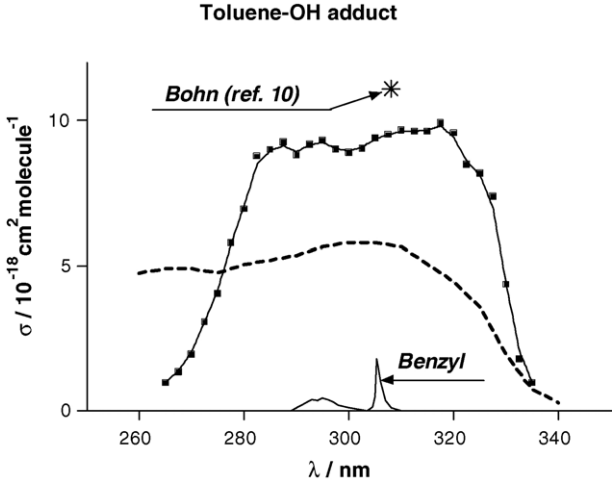

Fig. 3. UV absorption spectrum of the toluene-OH-adduct, *c*-$C_6H_5(CH_3)$-OH. Also shown are the cross-section measurement at 308 nm reported in reference [10] and the spectra roughly reproduced from the figures in reference [9]: *c*-$C_6H_5(CH_3)$-OH (dashed line) and benzyl radical (scaled by its yield). See comments in the text.

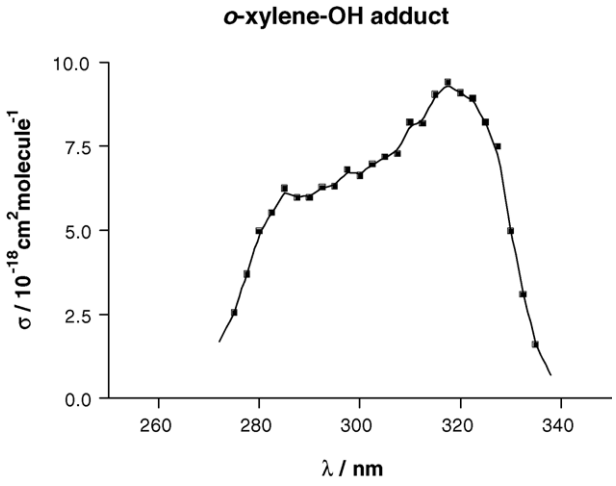

Fig. 4. UV absorption spectrum of the *o*-xylene-OH-adduct, 1,2-*c*-$C_6H_4(CH_3)_2$-OH.

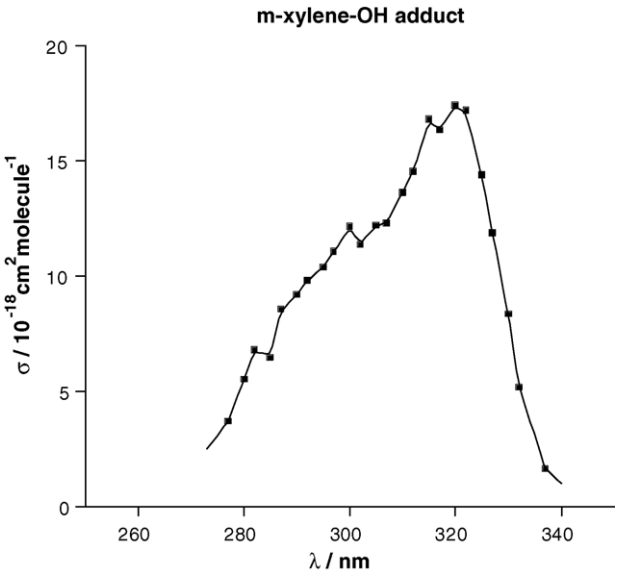

Fig. 5. UV absorption spectrum of the *m*-xylene-OH-adduct, 1,3-*c*-$C_6H_4(CH_3)_2$-OH.

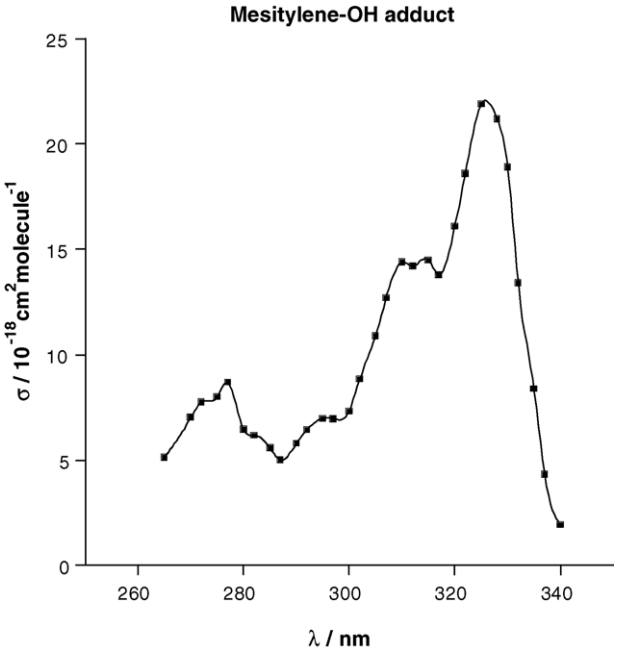

Fig. 7. UV absorption spectrum of the mesitylene-OH-adduct, 1,3,5-*c*-$C_6H_3(CH_3)_3$-OH.

for the *p*-xylene-OH-adduct, somewhat similar to the case for the benzene-OH-adduct [5,6], whereas the reverse situation is observed for the *o*-xylene-OH, *m*-xylene-OH and mesitylene-OH-adducts. For the toluene-OH-adduct both absorption bands are nearly equal in magnitude. It should be noted that in all cases absorption cross-sections are fairly high, with maximum values in the range $(0.9–2.2) \times 10^{-17}$ cm^2 molecule^{-1}.

Uncertainties in the cross-sections essentially result from the determination of radical concentrations in the experiments and from the determination of the base line of the transient absorption signals (which is complicated by the constant absorption generated by the laser excitation of the aromatic). The OH-adduct concentration is obtained by simulation of the experiments employing an initial OH concentration determined by calibration (which is equal to the initial $[C_2H_5O_2]$ generated under the same condition of OH radical precursor concentration) and from the rates of the various reactions consuming OH,

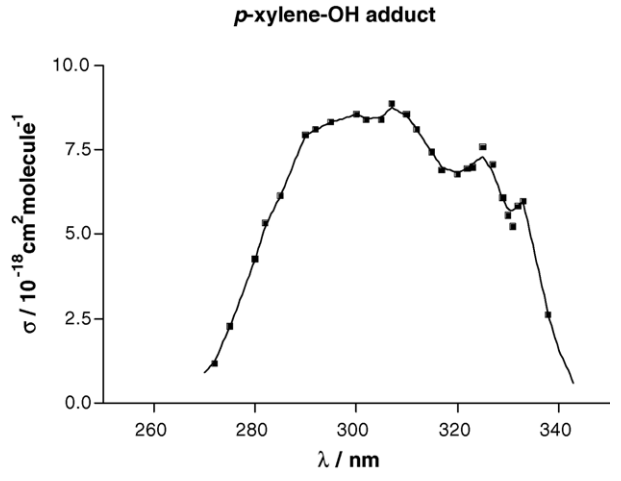

Fig. 6. UV absorption spectrum of the *p*-xylene-OH-adduct, 1,4-*c*-$C_6H_4(CH_3)_2$-OH.

principally, reactions (2) and (6), and, to a lesser extent, reactions (3), (7) and (10). Despite reaction (2) being dominant, errors in rate constants, and in concentrations of the species involved, resulted in an estimated uncertainty of the aromatic-OH-adduct concentration of around 15%. The error in the reference cross-section of $C_2H_5O_2$ is of the order of 5%. As indicated above, the base line of decay traces was assumed to be equal to the residual absorption measured at long reaction times, where radicals have all recombined. This was based on the observation that the residual absorption was nearly equal to the constant absorption obtained by the laser excitation of the aromatic compound in the absence of H_2O_2 (only extremely small, and fast decaying, transient absorptions could be seen under such conditions and hence were neglected). The residual absorption was small in the case of the *p*-xylene-OH-adduct, as shown in Fig. 1, but could be significantly larger (up to three to four times) in the case of other aromatics and under different experimental conditions. Absorbing products from radical recombination reactions may also have contributed to the residual absorption. This could not be clearly characterised, however, but nevertheless, may have contributed to the experimental error. It should again be emphasised that the decay traces recorded were reasonably well simulated with the reaction mechanism given in Table 1, using realistic values for the rate constants of radical–radical reactions. This indicates that large errors in determining the absorption baseline did not occur. The corresponding error in the aromatic-OH-adduct concentration is estimated to be around 10–15%. Thus, a global uncertainty of the order of 20–25% is estimated and this reflects the difficulty in making the present measurements.

To date, very few data have been reported in the literature, which can be compared to the present results. Only two investigations have been reported concerning the toluene-OH-adduct [9,10]. The single-wavelength absorption cross-section

measurement (308 nm) of Bohn [10] is 15% larger than that measured in this work (Fig. 3), but, given the experimental uncertainties, the agreement is reasonable. A spectrum of the toluene-OH-adduct has also been reported by Markert and Pagsberg [9] which exhibits a similar shape in the long wavelength part ($\lambda > 300$ nm) but with cross-section values nearly half of those measured in this work. Significant differences in the shape of the spectra are evident at shorter wavelengths (see Fig. 3). The differences can probably be explained by the contribution of other absorbing species produced by pulse radiolysis in the study of Markert and Pagsberg. These may include benzyl radicals, H-toluene-adduct species and, perhaps, other unidentified species. It can be seen in Fig. 3 that the sharp absorption line of the benzyl radical, at 305.3 nm, does not appear in our spectrum. Several reasons can be given to account for this: the spectral resolution used in this investigation is lower than that employed in ref. [9]; none of our experiments corresponded in wavelength to the maximum of this absorption line; the small contribution expected for this benzyl absorption may be hidden by a small minimum in the *c*-$C_6H_5(CH_3)$-OH spectrum at this wavelength.

The addition of OH to the ring of the methyl-substituted benzenes investigated in this work can yield different isomers of the aromatic-OH-adducts, according to the relative position of the attached OH-group and the methyl-group(s). For example, four isomers of the toluene-OH-adduct can be produced, corresponding to OH addition at *ipso*-, *ortho*-, *meta*- or *para*-positions. In contrast, only two isomers can be obtained in the cases of *p*-xylene and mesitylene (addition at *ipso*- and *ortho*-positions). Thus, it is of interest to identify which isomers are preferentially formed by the addition of OH to the aromatics studied in the present investigation, in order to assign a particular spectrum to a specific (or dominant) isomer or a distribution of isomers. To this end, we have used the results of experimental measurements of yields of stable ring-retaining products of the OH-initiated oxidation of the aromatic hydrocarbons of interest (these data are essentially summarised in reference [13]) along with theoretical chemical methods to estimate which isomers are preferentially formed.

Density functional theory (DFT) calculations were carried out using the B3LYP/6-31G(d) method in order to obtain chemical energies, and these were then used in transition state theory (TST) calculations to obtain kinetic data. A more detailed description of such calculations has been given in a preceding publication [16]. OH addition to aromatics involves the formation of a pre-reactive complex, as shown in theoretical studies of the formation of the benzene-OH-adduct [18] and of the toluene-OH-adduct [19]. Statistical methods were used in order to calculate decomposition rates of the toluene-OH pre-reactive complex for the determination of the branching ratios for the formation of OH-aromatic-adduct isomers [19].

Perhaps, the most informative experimental data are the structures and relative formation yields of the various phenol-type products (i.e. the ring-retaining, hydroxylated aromatic products of the addition reactions of OH with aromatic hydrocarbons) formed in the OH-initiated oxidation of the aromatics considered in the present study. Certain other oxidation products (for which formation yields have been reported, glyoxal and methylglyoxal, for example), which result from ring-fragmenting reaction pathways [13], may be formed from more than one possible isomer of a given OH-adduct, and thus do not provide any specific information about the initial radical-adducts from which they are formed. That said this is not true in the case of compounds bearing two adjacent methyl-groups (*o*-xylene in the present study) where biacetyl is produced, as discussed below. The phenol-type product (cresol in the example case of toluene) is formed according to reaction (5a)

$$c\text{-}C_6H_5(CH_3)\text{-}OH + O_2 \rightarrow c\text{-}C_6H_4(CH_3)\text{-}OH + HO_2 \quad (5a)$$

by direct abstraction of the H-atom attached to the carbon atom bearing the OH-group [16]. Thus, the structures and yields of phenolic-type products provide an indication of the site of the initial OH-addition assuming that the rate constants for reaction (5a) are similar for all isomers. That said, however, no indication of the occurrence of OH-addition at the *ispo*-position can be gained from such product studies due to the absence of an abstractable H-atom at this position of the ring.

OH addition at the *ipso*-position is generally not considered in the oxidation mechanisms of methyl-substituted aromatics [13] and yet no clear argument for this is found in the literature, except for the possible role of steric hindrance [20]. In the theoretical studies of Uc et al. [21,22], of the OH addition to toluene, it was concluded that both *ipso*- and *ortho*-isomers are the most stable and can be formed in significant yields. It should be noted, however, that the calculated energy differences between the isomer structures were within the calculation uncertainties (5–7 kJ mol^{-1}). In contrast to this latter, DFT calculations carried out in this laboratory indicate that the *ipso*-isomer is less stable than the other isomers (for OH-adducts of toluene and the other methyl-substituted aromatics), although again it should be noted that the energy differences are within calculation uncertainties. The present calculations also indicate that addition at the *ortho*-position is slightly energetically favoured over all other positions for toluene and for the other methyl-substituted aromatics.

In the case of toluene, the present calculations of kinetic parameters, using combined DFT and statistical methods, give yields of 54, 25, 18 and 3% for the *ortho*-, *para*-, *meta*- and *ipso*-isomers, respectively [19]. The low value obtained for the *ipso*-isomer is essentially due to a higher barrier on the reaction path from the pre-reactive complex to the OH-adduct. Experimentally determined cresol branching ratios are 0.12, 0.03 and 0.02 for *ortho*-, *para*- and *meta*-isomers, respectively [13], corresponding to a distribution of 70, 18 and 12%, respectively, for these phenol-type products if one neglects the *ipso*-isomer. The agreement between the calculated and experimentally determined distributions is reasonable, taking the fairly large uncertainties in both calculated and experimental values into account, and suggests that OH-addition at the *ipso*-position is of minor importance and can be neglected in this particular case. Thus, the observed distribution of cresol isomers provides a good indication of the isomer distribution of the toluene-OH-adducts, and hence their contribution to the transient absorption spectra observed. This also indicates that the

rate constant of reaction (5a) for the different OH-adduct isomers are similar.

Similar calculations could not be performed in the cases of other compounds, as they would involve prohibitively exaggerated computational time. The above results obtained for toluene suggest that the situation is similar for other compounds, the *ortho*-isomers of OH-adducts being the most abundant and addition at the *ipso*-position being a minor process. However, it has been observed in the particular cases of *o*-xylene and other methyl-substituted aromatics with two adjacent methyl-groups (1,2,3-trimethylbenzene and 1,2,4-trimethylbenzene), that biacetyl (butane-2,3-dione) is produced in relatively large yield, at least as large as the total yield of phenol-like products [13]. Now, considering the presently accepted ring-opening mechanism for α-dicarbonyl production [13], biacetyl formation can only result from OH-addition at the *ipso*-position. Thus, OH-addition at this site of the ring appears to be a major process in these particular cases. This is difficult to explain but may be due to the fact that addition at this type of *ipso*-site is favoured as it is also *ortho*- to an alkyl-substituent as the two methyl-substituents are adjacent.

In other cases, where the OH-addition at the *ipso*-site is of minor importance, the isomer distributions of the phenol-type products, obtained in the OH-initiated oxidation of methyl-substituted aromatics, provide an indication of the isomer distributions of the initial OH-adducts. These product distributions, taken from reference [13], are reproduced in Table 3 where it can be seen that carbon atoms, which are *ortho*- to a substituent methyl-group are favoured sites in the OH addition process. That said, however, as can be seen, other isomers may also be formed to a significant extent. In addition, as seen above for the particular case of the *o*-xylene precursor, the percentage for addition at the position, which is both *ortho*- and *ipso*- should be at least equivalent to that quoted for the simple *ortho*-position in Table 3. This means that the UV spectra reported in this work correspond to one or several isomers of OH-adducts for which an indicative distribution is given in Table 3. Nonetheless, they correspond to resultant spectra of the species obtained by OH-addition to the aromatic precursors considered, under conditions close to those encountered in the lower Earth's atmosphere.

Table 3
Average isomer distribution of phenol-type products obtained from the OH-initiated oxidation of toluene, xylenes and mesitylene under atmospheric conditions (from reference [13])

Precursor	Phenol-like product	Yield	Percentage of total phenol-like products
Toluene	2-Methyl phenol	0.12	70
	4-Methyl phenol	0.03	18
	3-Methyl phenol	0.02	12
o-Xylene	2,3-Dimethyl phenol	0.10	62
	3,4-Dimethyl phenol	0.06	38
m-Xylene	2,6-Dimethyl phenol	0.11	48
	2,4-Dimethyl phenol	0.09	39
	3,5-Dimethyl phenol	0.03	13
p-Xylene	2,5-Dimethyl phenol	0.13	100
Mesitylene	2,4,6-Trimethyl phenol	0.04	100

The percentage of corresponding initial OH-adduct isomers should be the same if one neglects addition at the *ipso*-position. In the case of *o*-xylene, however, the percentage of addition at the *ipso*-position is quite significant, at least equal to or larger than that quoted for the *ortho*-phenol-type product (see Section 4).

5. Conclusions

UV absorption spectra have been measured for five different methyl-substituted hydroxy-cyclohexadienyl radicals. Each spectrum exhibits a strong absorption band in the 260–340 nm wavelength region, as observed previously for other cyclohexadienyl-type radicals. The shape of the band and the maximum cross-section vary significantly from one radical to the next in the series of aromatic hydrocarbons investigated, and thus unfortunately, the present results cannot be extrapolated in order to estimate the UV absorption characteristics of radical adduct species formed in analogous reaction systems. Examination of the yields of ring-retaining, phenol-type oxidation products, identified in previous studies of OH-initiated oxidation of aromatics, combined with DFT calculations, indicate that one or more isomer of the OH-adducts may contribute to the observed absorption spectra. For all systems studied in the present investigation, isomers where the OH-group is *ortho*- or both *ortho*-/*ipso*- to a substituent methyl-group are indicated to be the most abundant, but other isomers may also be present to a significant extent (Table 3).

Acknowledgments

The authors acknowledge the EU for funding through the EXACT project (contract no. EVK2-CT-1999-00053). D.J. acknowledges the EU for postdoctoral funding with a Marie Curie fellowship and L.N.K. acknowledges the French CNRS for funding a 3-month stay at the University Bordeaux I.

References

[1] M.C. Sauer Jr., I. Mani, J. Phys. Chem. 74 (1970) 59–63.
[2] M.C. Sauer Jr., B. Ward, J. Phys. Chem. 71 (1967) 3971–3983.
[3] F. Berho, M.T. Rayez, R. Lesclaux, J. Phys. Chem. A 103 (1999) 5501–5509.
[4] E. Bjergbakke, A. Sillesen, P. Pagsberg, J. Phys. Chem. 100 (1996) 5729–5736.
[5] D. Johnson, S. Raoult, M.T. Rayez, J.C. Rayez, R. Lesclaux, Phys. Chem. Chem. Phys. 4 (2002) 4678–4686.
[6] S.Y. Grebenkin, L. Krasnoperov, J. Phys. Chem. A 108 (2004) 1953–1963.
[7] R. Zellner, B. Fritz, M. Preidel, Chem. Phys. Lett. 121 (1985) 412–416.
[8] B. Bohn, C. Zetzsch, Phys. Chem. Chem. Phys. 1 (1999) 5097–5107.
[9] F. Markert, P. Pagsberg, Chem. Phys. Lett. 209 (1993) 445–454.
[10] B. Bohn, J. Phys. Chem. A 105 (2001) 6092–6101.
[11] G.S. Tyndall, R.A. Cox, C. Granier, R. Lesclaux, G.K. Moortgat, M.J. Pilling, A.R. Ravishankara, T.J. Wallington, J. Geophys. Res. 106 (2001) 12157–12182.
[12] F.F. Fenter, P.D. Lightfoot, J.T. Niiranen, D. Gutman, J. Phys. Chem. 97 (1993) 5313–5320.
[13] J.G. Calvert, R. Atkinson, K.H. Becker, R.M. Kamens, J.H. Seinfeld, T.J. Wallington, G. Yarwood, The Mechanism of Atmospheric Oxidation of Aromatic Hydrocarbons, Oxford University Press, New York, 2002.
[14] N. Ikeda, N. Nakashima, K. Yoshihara, J. Phys. Chem. 88 (1984) 5803–5806.

[15] H. Hiratsuka, T. Okamura, I. Tanaka, Y. Tanisaki, J. Phys. Chem. 84 (1980) 285–289.
[16] S. Raoult, M.T. Rayez, J.C. Rayez, R. Lesclaux, Phys. Chem. Chem. Phys. 6 (2004) 2245–2253.
[17] W.B. DeMore, S.P. Sander, D.M. Golden, R.F. Hampson, M.J. Kurylo, C.J. Howard, A.R. Ravishankara, C.E. Kolb, M.J. Molina, Chemical Kinetics and Photochemical Data for Use in Stratospheric Modeling, Evaluation No. 12, Jet Propulsion Laboratory Pasadena, 1997.
[18] I.V. Tokmakov, M.C. Lin, J. Phys. Chem. A 106 (2002) 11309–11326.
[19] S. Raoult, Ph.D. Thesis, University Bordeaux I, 2003.
[20] J.M. Andino, J.N. Smith, R.C. Flagan, W.A. Goddard III, J.H. Seinfeld, J. Phys. Chem. 100 (1996) 10967–10980.
[21] V.H. Uc, I. Garcia-Cruz, A. Hernández-Laguna, A. Vivier-Bunge, J. Phys. Chem. A 104 (2000) 7847–7855.
[22] V.H. Uc, I. Garcia-Cruz, A. Grand, A. Vivier-Bunge, J. Phys. Chem. A 105 (2001) 6226–6231.
[23] A.A. Boyd, P.M. Flaud, N. Daugey, R. Lesclaux, J. Phys. Chem. A 107 (2003) 818–821.
[24] A.A. Boyd, E. Villenave, R. Lesclaux, Atmos. Environ. 37 (2003) 2751–2760.